

Earth X-ray albedo for CXB radiation in the 1-1000 keV band

E. Churazov^{1,2}, S. Sazonov^{1,2}, R. Sunyaev^{1,2}, M. Revnivtsev^{1,2}

¹ *Max-Planck-Institut für Astrophysik, Karl-Schwarzschild-Strasse 1, 85741 Garching, Germany*

² *Space Research Institute (IKI), Profsoyuznaya 84/32, Moscow 117810, Russia*

7 February 2020

ABSTRACT

We present calculations of the Cosmic X-ray background (CXB) reflection by the Earth atmosphere in the 1-1000 keV range and compare it with the reflection by the Moon and the Sun. The calculations use realistic chemical composition of the Earth atmosphere and include all relevant physical processes. An analytic approximation to the Earth X-ray albedo is provided, which should be accurate down to few percent level in the range from few keV up to few hundred keV.

Key words:

1 INTRODUCTION

Having a mass column density of $\sim 10^3 \text{ g cm}^{-2}$ at the sea level the Earth atmosphere completely blocks X-rays from celestial sources. At the same time outer layers of the Earth atmosphere reflect part of the incident X-ray photons due to the Compton scattering. The physical picture is very similar to the well studied case of the reflection from a star surface (e.g. Basko, Sunyaev & Titarchuk, 1974) or an accretion disk (e.g. George & Fabian, 1991) except for the different chemical composition of the reflection medium. The Earth reflection albedo peaks at ~ 60 keV and decline towards lower or higher energies.

The reflection of X-rays by the Earth atmosphere is important for e.g. evaluation of the echo produced by Gamma-ray bursts (Willis et al., 2005) or for CXB studies. This work was particularly initiated by the recent INTEGRAL observations of the Earth (Churazov et al., 2006) aimed at determining the CXB flux normalization near the peak of the luminosity distribution (i.e. around 30-40 keV).

Below we use the term “albedo” for the ratio of the flux reflected by the Earth disk at a given energy to the CXB flux at the same energy and coming from the same area. Since photons change the energy during Compton scattering and fluorescence, the albedo depends not only on energy, but also on the overall shape of the input spectrum. If the shape of the incident spectrum is not known then the Green function describing the reflection of monochromatic radiation has to be calculated (as was done in White, Lightman & Zdziarski, 1998). The convolution of the incident spectrum with the Green function produces the reflected spectrum. For our purposes the shape of the input spectrum is fixed and the above definition of the albedo is sufficient.

2 THE EARTH ATMOSPHERE MODEL

According to the standard model of the Earth atmosphere (see e.g. <http://www.spennis.oma.be/spennis>) a uniform chemical composition is a reasonably good approximation for the altitudes below ~ 90 km (the so-called “homosphere”). The relative chemical composition (by volume) of various species in the homosphere is $\text{N}_2 - 0.781$, $\text{O}_2 - 0.209$ and $\text{Ar} - 0.0093$. The uniformity of the chemical composition is maintained by the vertical winds and turbulent mixing. Above 90 km the chemical composition starts to vary with the altitude with lighter elements playing increasingly more important role. The temperature and the ionization state of the medium also vary substantially at high altitudes. However the mass column density of the atmosphere above 90 km is of order of only $\sim 10^{-3}$ g. Such low column densities can affect the X-ray albedo only at the lowest end of the considered energy range (around 1 keV) where the albedo is very small anyway. We therefore choose to neglect the more distant layers of the atmosphere.

The whole atmosphere has a very large optical depth at any energy of interest here (from 1 keV up to ~ 10 MeV). This ensures that any characteristic length scale of the problem (e.g. length scale corresponding to a unit optical depth at a given energy in the range from 1 keV up to 10 MeV) is of order of (or smaller) than the scale height of the atmosphere. All these characteristic length scales are much smaller than the Earth radius and a plane parallel atmosphere should be a reasonably good approximation. The vertical structure of the atmosphere can then be ignored and the atmosphere can be modeled as a plane parallel and uniform slab of matter (see e.g. Mihalas, 1978). In simulations the column density of the slab was set to a large value of ~ 1000 g so that the

slab illuminated from one side is effectively equivalent to a semi-infinite medium.

3 PHYSICAL PROCESSES

The following processes have been included in the simulations: photoelectric absorption, Rayleigh and Compton scattering and fluorescence. An additional process - electron-positron pair creation - takes place for the photon energies exceeding $2 \times m_e c^2 = 1022$ keV. For our purpose (the atmospheric albedo for CXB radiation in the 1-1000 keV energy band) the contribution of this process is very small. This contribution was evaluated using GEANT package (GEANT Collaboration, 2003) and was found to be less than 1 per cent across the 200-1000 keV band, excluding 511 keV line. In the rest of the paper we neglect this process.

The photoelectric absorption was calculated using the data and approximations of Verner & Yakovlev 1995 and Verner et al., 1996. For fluorescence we use the energies and yields from Kaastra & Mewe 1993.

The Compton and Rayleigh scattering is the most important process for this model. We used the same sources of information as is used in the GLECS package (Kippen, 2004) of the GEANT code (GEANT Collaboration, 2003). Namely the Livermore Evaluated Photon Data Library (EPDL, see Cullen, Perkins & Rathkopfand 1990) and the free electron Klein-Nishina formula are used to calculate total cross sections and the angular distribution of scattered photons for each element. The total cross sections for photoelectric, Compton and Rayleigh scatterings are shown in Fig.1. Unlike the case of a typical interstellar medium (ISM), composed from hydrogen, helium and small admixture of heavier elements, the Earth atmosphere is composed of heavier elements. This difference in composition has two important consequences. Firstly, the photoabsorption cross section exceeds the scattering cross section up to the energy of ~ 30 keV. Secondly, in contrast to the hydrogen dominated ISM, where total cross section is constant at low energies, for the atmospheric composition the Rayleigh scattering substantially increases the total scattering cross section below 10-20 keV (up to factor of almost 10 at 1 keV).

For Compton scattering an additional smearing of the scattered photon energy due to the distribution of bound electrons over momentum is accounted for using the data on the ‘‘Compton profile’’ from Biggs, Mendelsohn & Mann 1975. Unlike the case of a usual ISM, where Compton profile can produce interesting changes in the spectral shape of the fluorescent lines (Sunyaev & Churazov, 1996) for the reflection by air these effects are less important because at the energies of interesting fluorescent lines (e.g. for K_α line of argon at 2.96 keV) the photoabsorption strongly dominates the Compton scattering. The CXB itself does not have any sharp features in the spectrum which could make the effect of smearing in the reflected spectrum important. Nevertheless for completeness we include this effect in the simulations.

When modeling the scattering process the two nitrogen or oxygen atoms, composing N_2 or O_2 molecule, were considered as independent atoms. We therefore underestimating the cross section for forward scattering by a factor of 4. The characteristic range of scattering angles θ for which this additional increase of the the cross section is important can be

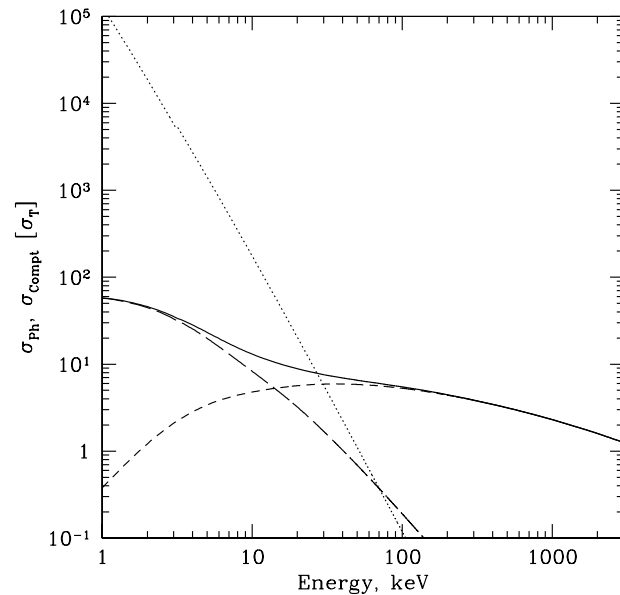


Figure 1. Adopted cross sections for photoelectric absorption (dotted line), Compton (short dash) and Rayleigh (long dash) scattering in air. Solid line shows the sum of the Compton and Rayleigh scattering cross sections. All cross sections are given in units of σ_T per atom. The nitrogen and oxygen atoms composing N_2 or O_2 molecules are treated as independent atoms. An additional increase of the Rayleigh scattering cross section (below 2-3 keV) due to the N_2 and O_2 molecules is neglected.

estimated from the condition $2\pi\theta\frac{R}{\lambda} \ll 1$, where R is the inter-atomic distance and λ is the wavelength of the photon. For a hydrogen molecule this characteristic angle is of order of 30-40 degrees for ~ 6 keV photons (Sunyaev, Uskov, Churazov, 1999) and increase of the total cross section is important below 3-4 keV. The inter-atomic distance for N_2 and O_2 is of order of 1.5 \AA , i.e. factor of two larger than the inter-atomic distance in the hydrogen molecule. Accordingly the total cross section will change significantly at only at energies as low as ~ 2 -3 keV. As is mentioned above the albedo at such energies is very low. In the rest of the paper these effects are neglected.

4 MODEL

We model the Earth atmosphere reflection via the Monte-Carlo method (see e.g. Pozdnyakov, Sobol & Sunyaev, 1983). For a given input spectrum $S_0(E)$ a logarithmic energy grid (with energy increasing by a factor of 1.01 between successive cells) is selected. For each cell of the grid an initial photon energy E_i is sampled randomly within the energy boundaries of the cell. The distribution of the input photons over angles follows the μ law, where $\mu = \cos\theta$ and θ is the angle between the input photon direction and the normal to the surface of the atmosphere. This distribution corresponds to the case of an element of the plane surface exposed to isotropic radiation from one side. Each input

photon is assigned an initial weight $w = 1$. On each step the total cross section at a current photon energy E is evaluated for all processes, the probability p of the photon escaping the slab is calculated and the value of $p \times w \times S_0(E)$ is added to the corresponding energy bin of the output spectrum. The weight of the photon is decrease by the factor $(1 - p)$ and the position of the next interaction is sampled. The relative contribution of the photoelectric absorption p_{PH} to the total cross section is used to decide if absorption or scattering takes place. In case of photoelectric absorption further decision is made if fluorescent photon is emitted (comparing weights of absorption cross sections and fluorescent yields for a set of shells). If fluorescent photon is emitted then the process continues with the new random photon direction and the new photon energy, which is equal to the fluorescent line energy. If scattering is picked instead, then the weight of the photon is reduces by a factor $(1 - p_{PH})$. A particular type of interaction (Compton or Rayleigh scattering) and a particular element (N, O or Ar) is then randomly selected according to their relative contribution to the total cross section. A new photon angle and energy are then sampled with account for relevant form factors for a given element and the whole process repeats. Once the weight of the photon drops below 10^{-7} the process stops and a new input photon from the same energy cell is selected. A new photon is also selected if the photon energy drops below 0.1 keV. Once N photons are drawn from the same cell of the energy grid the whole procedure is repeated for the next energy cell. Finally the spectra are divided by N producing the properly normalized reflected spectra.

The parameters of the energy grid and the number of photons drawn for each energy cell are tuned in such a way that the uncertainties in the final reflected spectra over the energy range of interest are small. For the albedo calculations we use $N = 20000$ making total number of photons played over whole energy range of about $2 \cdot 10^7$.

5 SIMULATIONS

As a starting point we set the shape of the input spectrum $S_0(E)$ to the broad band CXB spectrum approximation suggested by Gruber et al. (1999). Namely:

$$S_{CXB}(E) = \begin{cases} 7.877 E^{-0.29} e^{-E/41.13} & 3 < E < 60 \text{ keV} \\ \begin{cases} 0.0259 (E/60)^{-5.5} + \\ 0.504 (E/60)^{-1.58} + \\ 0.0288 (E/60)^{-1.05} \end{cases} & E > 60 \text{ keV} \end{cases} \quad (1)$$

Where $S_{CXB}(E)$ is in units of $\text{keV}/\text{keVcm}^{-2}\text{s}^{-1}\text{sr}^{-1}$.

5.1 Maximal energy in the input spectrum

Since we are interested in the reflected spectrum over a broad energy range (up to ~ 1 MeV) and at these energies the change of the photon energy due to recoil effect is large, it is important to take into account photons with the initial energy sufficiently larger than 1 MeV. Fig.2 shows the effect on the reflected spectrum of varying the maximal energy E_{max} in the input spectrum. The sequence of spectra shown corresponds to $E_{max}=0.15, 0.2, 0.3, 0.4, 1, 3, 5$ and 9 MeV. As is clear from this figure, in order to reproduce the shape

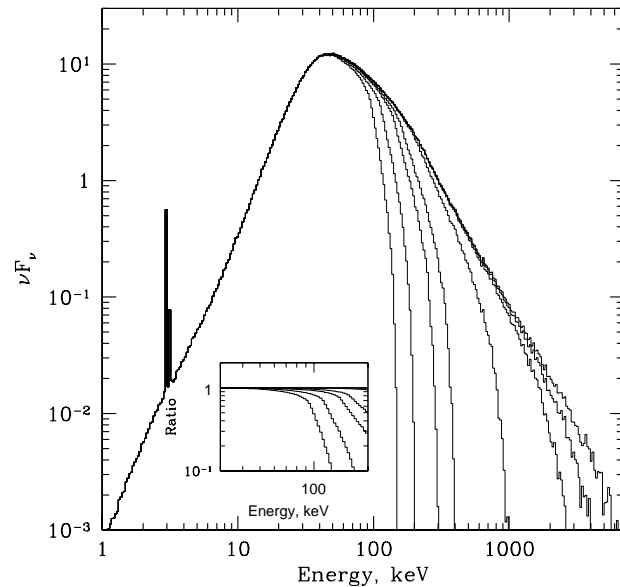


Figure 2. Dependence of the reflected spectrum on the high energy cutoff E_{max} in the input spectrum. The spectra shown correspond to $E_{max} = 0.15, 0.2, 0.3, 0.4, 1, 3, 5$ and 9 MeV. The inset shows the ratio of the spectra with a given E_{max} to the spectrum with $E_{max} = 9$ MeV near the maximum of the reflected spectrum.

of the reflected spectra with a reasonable accuracy (for the shape of the illuminating spectra not much different from eq.1) one needs to use a broad energy range up to at least 5-9 MeV. In the subsequent calculations we use $E_{max}=9$ MeV.

The inset in Fig.2 shows the part of the reflected spectrum near its maximum. It shows that i) the reflected spectrum near the peak of the CXB spectrum (~ 30 -50 keV in the νF_ν units) is not sensitive to the details of the incident spectrum above 150 keV. Near 100 keV and above the recoil effect is much more important and shape of the reflected spectrum become sensitive to the extrapolation of the incident spectrum to higher energies.

5.2 The shape of the input spectrum

Of course the reflected spectrum depends both on the shape and normalization of the illuminating spectrum. Since we are mainly interested in the effective atmospheric albedo (i.e. the ratio of the reflected and input spectra) the dependence on the normalization disappears, but the shape of the input spectrum still affects the behavior of the albedo at the energies larger than 20-30 keV. Fig.3 shows the atmospheric albedo for different shapes of the input spectra. The thick solid line shows our reference CXB input spectrum and the corresponding albedo. For comparison we show a set of input power law spectra with photon indices $\Gamma = 2.2, 2.5$ and 2.8 and the corresponding albedo.

One can see that below 20-30 keV the shape of the albedo (as a function of energy) does not depend on the

properties of the input spectrum. This is of course expected since in this regime i) photoelectric absorption dominates and therefore only first scattering is important and ii) the change of energy due to recoil effect is small. For these energies it is easy to write the expression for the albedo through the ratio of the absorption and scattering cross sections. Namely, in a single scattering approximation the reflected emission at an energy E_1 can be written as:

$$I_1(E_1) = \int I(E, \mathbf{n}) e^{-\sigma(E)\rho z/\mu - \sigma(E_1)\rho z/\mu_1} \rho \sigma_p(E, E_1, \mu_s) \frac{1}{\mu} dz dE d\Omega d\Omega_1 = \int I(E, \mathbf{n}) \frac{\sigma_p(E, E_1, \mu_s)}{\frac{\sigma(E)}{\mu} + \frac{\sigma(E_1)}{\mu_1}} \frac{1}{\mu} dE d\Omega d\Omega_1,$$

where $I(E, \mathbf{n}) = I(E)\mu$ is the incident spectrum, $\sigma(E)$ is the total cross section for all processes, $\sigma_p(E, E_1, \mu_s)$ is the differential cross section for the process which is responsible for reflected radiation (e.g. Compton scattering or photoelectric absorption followed by the emission of a fluorescent photon), z is the vertical coordinate and μ is the cosine of the angle between photon direction the vertical direction, and μ_s is the cosine of the scattering angle. At low energies the recoil effect is weak and the energy of the photon is conserved $E_1 = E$. One can therefore set $\sigma_p(E, E_1, \mu_s) = 1/2r_e^2(1 + \mu_s^2)S(\mu_s, E)\delta(E - E_1)$, where r_e is the classic radius of the electron and $S(\mu_s, E)$ is the form factor. Thus the reflected spectrum is

$$I_1(E_1) = I(E_1) \frac{1/2r_e^2}{\sigma(E_1)} \int S(\mu_s, E_1)(1 + \mu_s^2) \frac{\mu\mu_1}{\mu + \mu_1} d\Omega d\Omega_1. \quad (3)$$

The approximation should work at energies below ~ 20 keV, where only the first scattering is important. The expression 3 can be readily integrated for a known form factor.

For a pure Thomson scattering (on free and cold electrons) ($S(\mu_s, E) = 1$) the expression for the reflected spectrum further simplifies to:

$$I_1(E_1) = 0.65 \times I(E_1) \frac{\sigma_s(E_1)}{\sigma_s(E_1) + \sigma_{ph}(E_1)}, \quad (4)$$

where $\sigma_s(E_1)$ is the total scattering cross section and $\sigma_s(E_1) + \sigma_{ph}(E_1)$ is the sum of the scattering and photoabsorption cross sections. Such a simple approximation works reasonably well up to 20 keV (see Fig.3). The single scattering approximation is certainly valid in this regime. The reason for the discrepancy is the large contribution of the Rayleigh scattering in air to the total scattering cross section. Since Rayleigh scattering is mostly contributing to small angle scattering, it's contribution to the scattered flux is overestimated by eq.4.

At energies higher than 30 keV the uncertainty in the photon index of the incident spectrum directly translates into the moderate changes in the albedo. E.g. at the energy of ~ 100 keV the change in the photon index of the incident spectrum from $\Gamma = 2.2$ to 2.8 corresponds to the $\sim 25\%$ change in the albedo. For a particular problem of measuring the CXB signal by the Earth occultation the most important quantity is $(1 - A(E))$, where $A(E)$ is the Earth albedo. This quantity characterizes the modification of the CXB signal occulted by the Earth due to the reflection of the Earth atmosphere. Given that the maximal value of the albedo

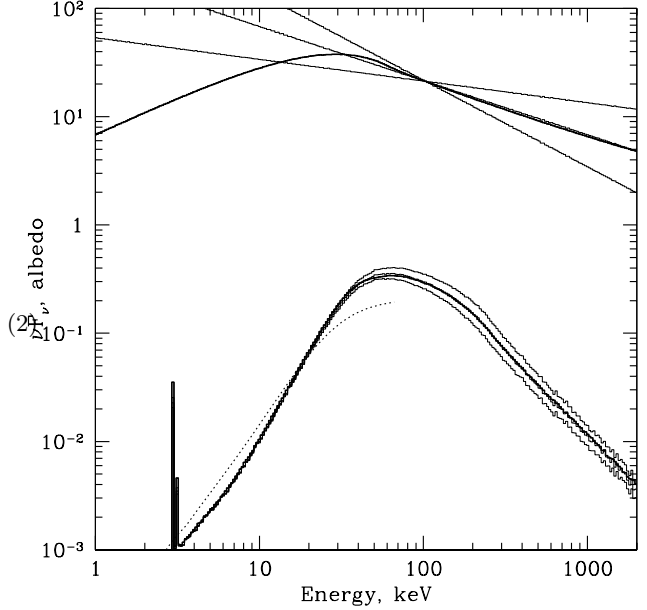


Figure 3. Dependence of the albedo on the shape of the incident spectrum. The input spectra (shown in the upper part of the plot) are the power laws with photon indices $\Gamma = 2.2, 2.5$ and 2.8. For comparison the CXB spectrum is shown by the thick solid line. In the lower part of the plot the albedos calculated for these input spectra are shown. The thick line shows the albedo for CXB spectrum. The dotted line shows a simple calculation of the albedo according to equation 4.

is $\sim 0.3-0.4$, the 25% changes in the albedo correspond to changes in $(1 - A(E))$ of less than 10%.

5.3 Fluorescent lines

The energies of the fluorescent lines for N, O and Ar are given in Table 1. All these energies fall in the regime where photoelectric absorption is a dominant process and only first scattering matters. The equivalent width of the fluorescent line is the ratio of the line flux and the scattered continuum. For the line flux we set in eq.2 the cross section $\sigma_p(E, E_1, \mu_s) = \sigma_{ph,sh}(E)\delta(E_1 - E_l)Y_l/4\pi$, where $\sigma_{ph,sh}(E)$ is the photoabsorption cross section for a given shell, E_l is the line energy and Y_l is the fluorescent yield. The line flux is then

$$I_l = \int I(E) \frac{\sigma_{ph,sh}(E)Y_l}{4\pi} \frac{1}{\frac{\sigma(E)}{\mu} + \frac{\sigma(E_l)}{\mu_1}} dE d\Omega d\Omega_1 = \int I(E) \frac{\sigma_{ph,sh}(E)Y_l 2\pi}{3\sigma(E)^2\sigma(E_l)^2} \times \{ \sigma(E)\sigma(E_l)(\sigma(E) + \sigma(E_l)) + \sigma(E_l)^3 \log \left(\frac{\sigma(E_l)}{\sigma(E) + \sigma(E_l)} \right) + \sigma(E)^3 (\log(\sigma(E)) - \log(\sigma(E) + \sigma(E_l))) \} dE. \quad (5)$$

The above expression can be readily integrated and the equivalent width evaluated as the ratio of eqn.5 and 3 or

Table 1. Equivalent width of the fluorescent lines.

Element	Line energy (keV)	Yield	EW, keV
N, K_{α}	0.39	0.0060	94.3
O, K_{α}	0.52	0.0094	7.85
Ar, K_{α}	2.96	0.112	2.61
Ar, K_{β}	3.19	0.01	0.27

4. The expected values of the equivalent width are given in Table 1. These values agree well with the results of the simulations.

5.4 Angular dependence in the reflected emission

The dependence of the emerging spectrum on the viewing angle is illustrated in Fig.4. The thick lines show the incident spectrum and the reflected spectrum integrated over all angles. Below the integrated reflected spectrum we show the emerging spectra for $\mu=0.9,0.7,0.5,0.3,0.1$ (from top to bottom around 30-50 keV), where $\mu = \cos(\theta)$ - is the angle of outgoing radiation with respect to the normal to the surface. One can see that the behavior of spectra at low and high energies differs dramatically. For instance at high energies the dominant contribution to the total reflected spectrum is due to the photons emerging at small angle to the surface. This can be easily understood since for the photons emerging almost along the normal, the smallest possible scattering angles are of order of 90 degrees. This implies large recoil effect. For instance for scattering by 90 degrees the energy of the scattered photon does not exceed 511 keV. Thus at energies above 511 keV the photons scattered only once do not contribute to the spectrum emerging along the normal to the surface. This causes the drop in the spectrum at high energies. On the contrary for the spectra emerging at small angle to the surface there is always a contribution from the photons scattered only once (by a small angle). This effect gives rise to an angular dependence of the emerging spectra, especially prominent at high energies as shown in Fig.5. In this figure we show the dependence of the flux on cosine of the viewing angle μ for two energy bands: 30-40 keV (solid line), 200-300 keV (dashed line) and 500-600 keV (dotted line). The fluxes are divided by μ so that for the black body type of the emerging radiation (the so-called $\cos(\theta)$ law) the curves should be flat. Instead we see that at high energies the flux divided by μ grows strongly towards small values of μ (small angles to the surface). This effect will cause a ‘‘limb brightening’’ for the observations of the Earth disk.

5.5 Impact of the chemical composition on the albedo

The photoelectric cross section drops approximately as E^{-3} above the energy of the highest absorption edge present in a given compound (see Fig.1). The Compton scattering cross section on the contrary only slowly changes between 10 and 1000 keV. As a result for any realistic (for astrophysical conditions) chemical composition of the reflecting medium, above 100-200 keV the Compton scattering strongly dominates over the photoelectric absorption. This means that the

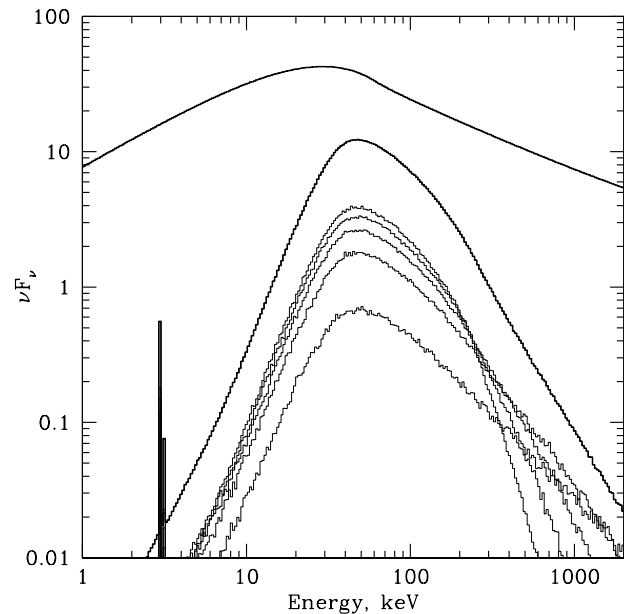


Figure 4. Dependence of the emerging spectrum on the cosine of the viewing angle. The top two curves show the incident spectrum and the emerging spectrum integrated over all angles. Lower curves show the emerging spectra for range of angles $\mu = 0.0-0.2$, $0.2-0.4$, $0.4-0.6$, $0.6-0.8$, $0.8-1.0$ (from bottom to top).

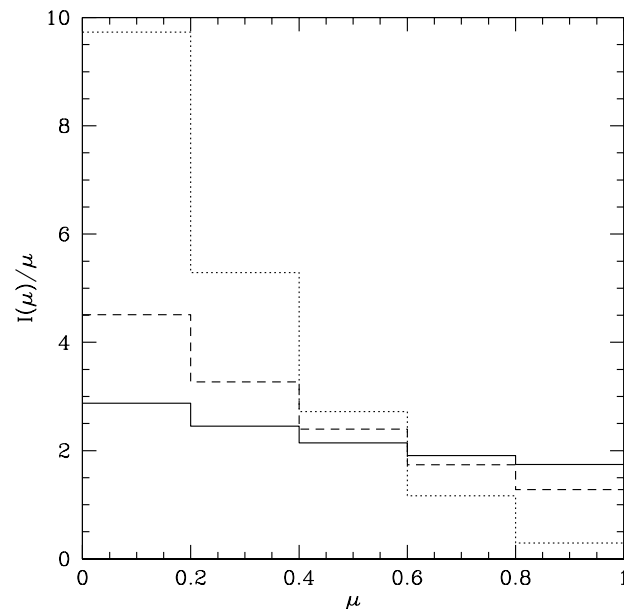


Figure 5. Dependence of the flux in the 30-40, 200-300 and 500-600 keV bands (solid, dashed and dotted curves respectively) on the cosine of the viewing angle μ . The fluxes are divided by μ and for a black-body type angular dependence the curves have to be flat.

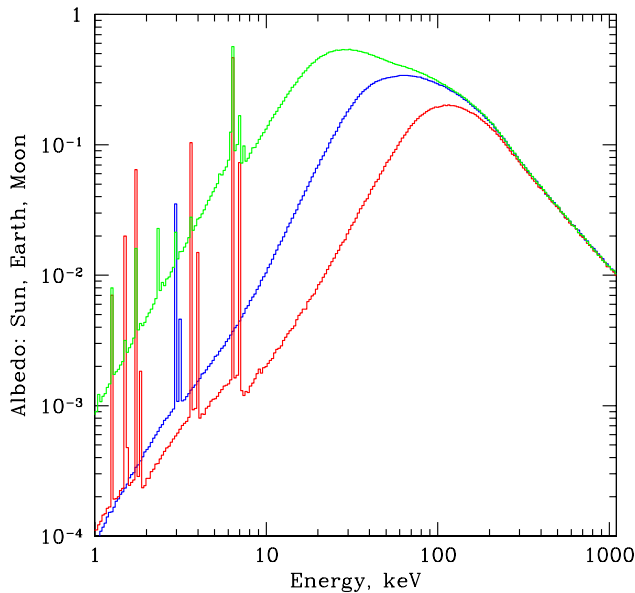


Figure 6. Albedo calculated for CXB spectrum and different chemical compositions: Solar photosphere (upper curve), Earth atmosphere (middle curve), Moon surface (bottom curve).

shape of the albedo above ~ 100 - 200 keV is not sensitive to chemical composition of the medium.

At low energies, on the contrary, the photoelectric absorption plays the dominant role and each material leaves its own imprints on the reflection albedo. This is illustrated in Fig.6 where the reflection albedo is shown for three markedly different chemical compositions. The uppermost curve corresponds to the Solar photospheric chemical composition, i.e. the standard hydrogen and helium dominated gas with small admixture of heavy elements. This “solar” albedo (peaks around 20-30 keV and the reflected spectrum has a very strong iron fluorescent line at 6.4 keV. The lowest curve was calculated assuming a chemical composition typical for the Moon surface - a mixture of O, Si, Fe, Ca, Al, Mg plus admixture of other elements. For this chemical composition the photoelectric absorption plays much greater role, the reflectivity of the surface at low energies is much smaller and the peak of the albedo is shifted to ~ 100 keV. The Earth atmosphere chemical composition corresponds to the intermediate case and the albedo also has the properties intermediate between the Sun and the Moon cases.

The albedo is of course smallest for the Moon case, since more heavy elements (compared to the Earth atmosphere or the Solar photosphere) dominate the chemical composition. From this point of view the Moon is a better screen for the CXB signal than the Earth. For the typical satellite orbit (in particular for INTEGRAL) the angular size of the Moon is $\sim 30'$ arcmin only (diameter) and the obscuration by the Earth has a very strong advantage in terms of the subtended solid angle.

Both the Moon and the Sun could produce reflection signals associated with the bright GRBs or other transient events. For instance, recently the Helicon instrument

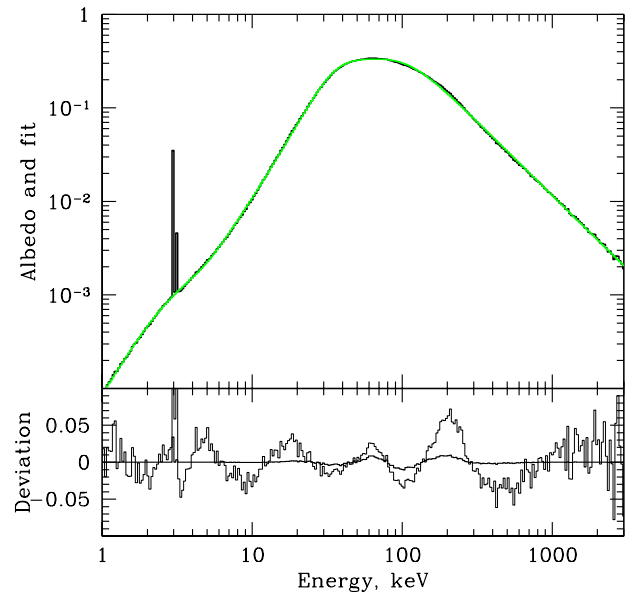


Figure 7. Comparison of the albedo $A(E)$ integrated over all angles (thick gray curve) and the analytic approximation (black curve). The thin curve in the lower panel shows the relative deviation of the simulated albedo and the analytic approximation. For the CXB studies more important is the absolute value of the difference between the simulated albedo and the analytic approximation. This difference is shown in the lower panel with the thick solid line. It is less than 1% at any energy in the 1-1000 keV range, except for the energy of the argon fluorescent line.

on board Coronas-F spacecraft detected the giant outburst from the soft gamma-ray repeater SGR1806-20 reflected by the Moon (Mazets et al., 2005). In this particular observation the repeater and the Sun were both occulted by the Earth and only the emission reflected by the Moon was detected. Should the mutual orientation of the objects be different the Sun could produce stronger (especially at energies below 100 keV) reflection signal.

6 DISCUSSION

The energy dependence of the Earth albedo (evaluated for the input spectrum with the shape according to eq.1 and ignoring the contribution of the fluorescent lines) can be approximated in the 1-1000 keV energy range by the following formula:

$$A(E) = \frac{1.22}{\left(\frac{E}{28.5}\right)^{-2.54} + \left(\frac{E}{51.3}\right)^{1.57} - 0.37} \times \frac{2.93 + \left(\frac{E}{3.08}\right)^4}{1 + \left(\frac{E}{3.08}\right)^4} \times \frac{0.123 + \left(\frac{E}{91.83}\right)^{3.44}}{1 + \left(\frac{E}{91.83}\right)^{3.44}} \quad (6)$$

As one can see from Fig.7 this approximation is accurate down to few percents in the 1-1000 keV energy range. For

an observer located at some distance D from the Earth the flux integrated over the full Earth disk will then be:

$$S_{obs}(E) = S_{CXB}(E)A(E)\Omega, \quad (7)$$

where Ω is the solid angle subtended by the Earth. The angular dependence of the emerging spectra is not important and the albedo has universal energy dependence as long as the full Earth disk is used. In particular the result does not depend on the distance D from the Earth. If however only part of the disk is seen or the efficiency of the telescope varies substantially across the Earth disk, then the albedo is no longer described by a universal function and has to be calculated taking into account angular dependence of emerging radiation. For the INTEGRAL observations (see specifics of these observations in Churazov et al., 2006) the equation 7 is a reasonable approximation when the Earth was well inside the instruments field of view.

In reality for the CXB studies the measured signal is the difference between the CXB signal obscured by the Earth and the reflected CXB flux. Since outer layers of the Earth atmosphere may be opaque at low energies and transparent at high energies the apparent angular “size” of the Earth Ω (see eq.7) does depend on energy. For instance the optical depth of unity is reached for line of sight having an impact parameter of $\sim R_e + 120$ km at the energy of 1 keV, where R_e is the Earth radius. For comparison at 30 keV and 1 MeV the corresponding impact parameter is $\sim R_e + 100$ and 60 km respectively. This effect limits the accuracy of our approximation - eq.7 - to $\sim 2\%$.

7 CONCLUSIONS

We calculated the Earth atmospheric albedo for the CXB radiation in the 1-1000 keV energy range. The albedo peaks around 60 keV with the maximum value of $\sim 35\%$. In the standard X-ray band (2-10 keV) the albedo is small and varies 0.05% to 1.3%. Around 1 MeV the albedo is of order of 1%. The equivalent width of the Ar K_α at 2.96 keV line is of order of 2.6 keV, but the net flux in the line is small. An analytic approximation of the albedo is provided. This approximation can be used to evaluate the albedo averaged over the whole Earth disk. If only part of the disk is observed then additional effects (like limb darkening/brightening for low and high energies respectively) have to be taken into account.

At high energies (above ~ 50 -100 keV) the Earth atmosphere becomes a powerful source of hard radiation induced by the interaction of Cosmic Rays with the atmosphere. Typical spectra of the atmospheric emission are calculate in Sazonov et al. 2006. The reflection of the CXB photons in this regime is of secondary importance.

The accuracy of the present calculations is sufficient for appropriate account for the CXB reflection by the Earth atmosphere during INTEGRAL observations of the Earth (Churazov et al., 2006).

REFERENCES

Basko M. M., Sunyaev R. A., Titarchuk L. G., 1974, A&A, 31, 249
 Biggs F., Mendelsohn L. B., Mann J. B., 1975, ADNDT, 16, 201

Geant4 Collaboration, et al., 2003, NIMPA, 506, 250
 George I. M., Fabian A. C., 1991, MNRAS, 249, 352
 Churazov E., et al., 2006, A&A, to be submitted
 Gruber D. E., Matteson J. L., Peterson L. E., Jung G. V., 1999, ApJ, 520, 124
 Cullen D. E., Perkins S. T., Rathkopf J. A. , "The 1989 Livermore Evaluated Photon Data Library (EPDL)," UCRL-ID-103424, Lawrence Livermore National Laboratory (1990).
 Kaastra J. S., Mewe R., 1993, A&AS, 97, 443
 Kippen R. M., 2004, NewAR, 48, 221
 Mazets E.P., et al., 2005, astro-ph/0502541
 Mihalas D., 1978, Stellar atmospheres, San Francisco, W. H. Freeman and Co.
 Pozdniakov L. A., Sobol I. M., Sunyaev R. A., 1983, ASPRv, 2, 189
 Sazonov S. Yu., et al., 2006, MNRAS, to be submitted
 Sunyaev R. A., Churazov E. M., 1996, AstL, 22, 648
 Sunyaev R. A., Uskov D. B., Churazov E. M., 1999, AstL, 25, 199
 White T. R., Lightman A. P., Zdziarski A. A., 1988, ApJ, 331, 939
 Willis D. R., et al., 2005, A&A, 439, 245
 Verner D. A., Ferland G. J., Korista K. T., Yakovlev D. G., 1996, ApJ, 465, 487
 Verner D. A., Yakovlev D. G., 1995, A&AS, 109, 125